HOLOGIC®
The Science of Sure

Powerful images.
Clear answers.

Manage Patient's concerns about Atypical Femur Fracture*

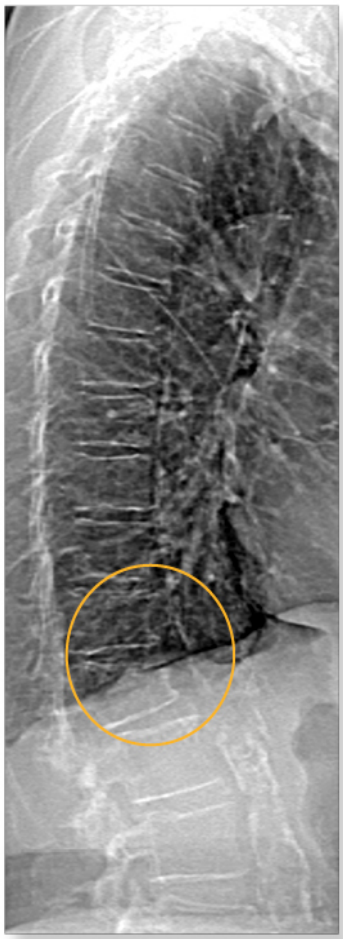

Vertebral Fracture Assessment – a critical part of a complete fracture risk assessment

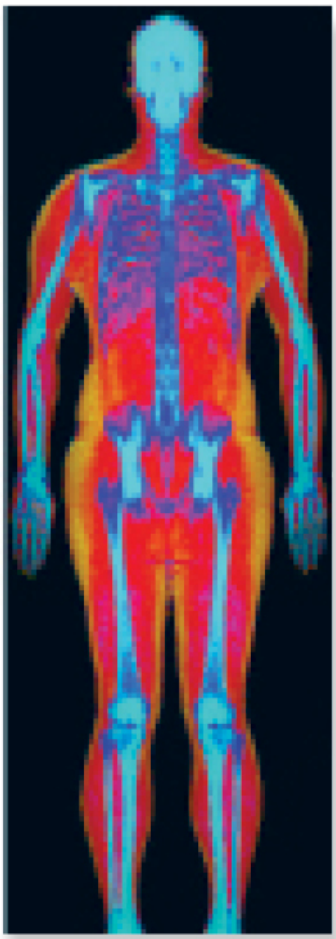

Advanced Body Composition® Assessment – the power to see what's inside

Contact your Hologic rep today at BSHSalesSupportUS@hologic.com

PAID ADVERTISEMENT

*Incomplete Atypical Femur Fractures imaged with a Hologic densitometer, courtesy of Prof. Cheung, University of Toronto

ADS-02018 Rev 003 (10/19) Hologic Inc. ©2019 All rights reserved. Hologic, Advanced Body Composition, The Science of Sure and associated logos are trademarks and/or registered trademarks of Hologic, Inc., and/or its subsidiaries in the United States and/or other countries. This information is intended for medical professionals in the U.S. and other markets and is not intended as a product solicitation or promotion where such activities are prohibited. Because Hologic materials are distributed through websites, eBroadcasts and tradeshows, it is not always possible to control where such materials appear. For specific information on what products are available for sale in a particular country, please contact your local Hologic representative.

www.hologic.com | dxaperformance.com | 1.800.442.9892

Check for updates

Glutamine metabolism in osteoprogenitors is required for bone mass accrual and PTH-induced bone anabolism in male mice

Running title: Glutamine metabolism in osteoprogenitors

Steve Stegen[a], Claire-Sophie Devignes[a], Sophie Torrekens[a], Riet Van Looveren[a], Peter Carmeliet[b-d] and Geert Carmeliet[a]

[a]Laboratory of Clinical and Experimental Endocrinology, Department of Chronic Diseases, Metabolism and Ageing, KU Leuven, Leuven, Belgium

[b]Laboratory of Angiogenesis and Vascular Metabolism, VIB Center for Cancer Biology, Leuven, Belgium

[c]Laboratory of Angiogenesis and Vascular Metabolism, Department of Oncology and Leuven Cancer Institute, KU Leuven, Leuven, Belgium

[d]State Key Laboratory of Ophtalmology, Zhongshan Ophtalmic Center, Sun Yat-Sen University, Guangzhou, China

Accepted Article

This article has been accepted for publication and undergone full peer review but has not been through the copyediting, typesetting, pagination and proofreading process which may lead to differences between this version and the Version of Record. Please cite this article as doi: 10.1002/jbmr.4219

This article is protected by copyright. All rights reserved.

Accepted Article

Corresponding Author:

Geert Carmeliet, M.D., Ph.D.

Laboratory of Clinical and Experimental Endocrinology, Department of Chronic Diseases, Metabolism and Ageing, KU Leuven

O&N1 Herestraat 49 bus 902, 3000 Leuven, Belgium

Tel.: 0032 16 330 731

Fax: 0032 16 330 718

e-mail: geert.carmeliet@kuleuven.be

Disclosures

The authors have nothing to disclose

This article is protected by copyright. All rights reserved.

Accepted Article

Abstract

Skeletal homeostasis critically depends on the proper anabolic functioning of osteolineage cells. Proliferation and matrix synthesis are highly demanding in terms of biosynthesis and bioenergetics, but the nutritional requirements that support these processes in bone-forming cells are not fully understood. Here, we show that glutamine metabolism is a major determinant of osteoprogenitor function during bone mass accrual. Genetic inactivation of the rate-limiting enzyme glutaminase 1 (GLS1) results in decreased postnatal bone mass, caused by impaired biosynthesis and cell survival. Mechanistically, we uncovered that GLS1-mediated glutamine catabolism supports nucleotide and amino acid synthesis, required for proliferation and matrix production. In addition, glutamine-derived glutathione prevents accumulation of reactive oxygen species and thereby safeguards cell viability. The pro-anabolic role of glutamine metabolism was further underscored in a model of parathyroid hormone (PTH)-induced bone formation. PTH administration increases glutamine uptake and catabolism, and GLS1 deletion fully blunts the PTH-induced osteoanabolic response. Taken together, our findings indicate that glutamine metabolism in osteoprogenitors is indispensable for bone formation.

Key words: osteoprogenitor, glutamine metabolism, biosynthesis, redox homeostasis, PTH

This article is protected by copyright. All rights reserved.

Accepted Article

Introduction

The adult skeleton is a highly dynamic tissue in which damaged or fatigued bone is continuously repaired through the coupled action of bone-resorbing osteoclasts and bone-forming osteoblasts [1]. During this process of bone remodeling, osteoprogenitors proliferate and differentiate into osteoblasts, which deposit extracellular matrix and subsequently mineralize it. These anabolic functions are critical for the preservation of bone mass, since a decrease in osteoblast function and/or number is associated with bone loss or reduced bone quality, as often seen upon ageing [2-5]. Current therapies that prevent bone loss predominantly halt bone resorption, whereas osteoanabolic drugs that increase bone mass are scarce. To date, only few bone anabolic therapies, including a derivative of parathyroid hormone (PTH; teriparatide) or an anti-sclerostin antibody (romosozumab), have reached clinical practice although the beneficial effects wane over time and adverse effects have been reported [6,7]. Understanding the mechanisms that govern the specific functions of osteogenic cells is therefore necessary to accelerate the development of novel bone anabolic therapeutics.

While the transcriptional factors and developmental signals that control osteoblast differentiation and function have been extensively studied [8,9], the metabolic features of osteolineage cells are only starting to be characterized. Like other anabolic cells, osteoprogenitors and osteoblasts rely on a continuous and sufficient supply of nutrients to meet the metabolic demands of proliferation, and extracellular matrix synthesis and mineralization. Moreover, these cells survive and function in a relatively hypoxic microenvironment [10], indicating that maintaining proper redox homeostasis is needed to avoid reactive oxygen species (ROS) accumulation [11]. To date, the vast majority of studies on intermediary osteoblast metabolism have focused on the utilization of glucose and fatty acids. Bone tissue takes up a substantial amount of postprandial glucose and lipids [12,13], which are consecutively catabolized in different metabolic pathways. The current

This article is protected by copyright. All rights reserved.

Accepted Article

understanding is that these nutrients, in basal conditions and in response to osteoanabolic stimuli such as Wnt family members (WNTs) or PTH, are used for energy generation [14-17], although a clear metabolic link between substrate catabolism and ATP production is still lacking. Moreover, it raises the question whether osteoblasts require additional nutrients to support other metabolic functions like biosynthesis and redox homeostasis.

A conceivable nutrient with diverse metabolic roles is glutamine, the most abundant amino acid in circulation [18]. Besides direct contribution to protein synthesis, glutamine is considered as an important energy source as well as a metabolic precursor for the synthesis of amino acids, nucleotides and the ROS scavenger glutathione [19-21]. A critical step to fulfill its metabolic functions is the conversion of glutamine to glutamate, which is primarily mediated by the enzyme glutaminase (GLS). While glutamine metabolism has been mostly studied in the context of cancer biology, recent reports have also suggested an important regulatory role in bone cells. Indeed, in skeletal stem cells glutamine metabolism is involved in osteogenic lineage specification [22], and in osteoblast progenitors WNT3A stimulates glutamine metabolism along with an increase in bone formation [23], although the underlying metabolic mechanisms that mediate these effects are not fully understood.

Here, we characterized the role of glutamine metabolism in early osteoblast progenitors during postnatal bone acquisition and PTH-induced bone formation. We demonstrate that loss of GLS1, the most expressed glutaminase isoform, in osteoprogenitors impairs bone mass accrual, and this phenotype is caused by a defect in biosynthesis and ROS-induced cell death. Moreover, we show that PTH treatment increases glutamine uptake and GLS1-dependent catabolism, which in turn is necessary to support the increase in osteoblast anabolism.

This article is protected by copyright. All rights reserved.

Accepted Article

Materials and methods

Animals

Deletion of GLS1 in osteoprogenitors and their descendants was obtained by crossing *Gls1*$^{fl/fl}$ mice (exon 1 was flanked by LoxP sites, mice were generated as described before [24]) with *Osterix* (*Osx*)-GFP:Cre transgenic mice [25]. *Osx*-GFP:Cre mice carry a tetracycline responsive element-controlled GFP:Cre fusion protein, and were treated with doxycycline (Dox) in the drinking water (50 mg/L Dox hyclate and 2% (wt/vol) sucrose (both from Sigma-Aldrich, Belgium)) from conception until weaning to prevent Cre-mediated recombination in *Osx*-positive cells. Genotypes were determined by PCR analyses of genomic DNA extracted from mouse-digit snips using the following primers: Cre forward, 5′-CCCGCAGAACCTGAAGATG-3′ and reverse, 5′-GACCCGGCAAAACAGGTAG-3′; LoxP *Gls1* allele forward, 5′-CACACCCCGTCCCGGACTTTTTC-3′ and reverse, 5′-AGAGCAGCTCCCGTAGCATC-3′. *Gls1*$^{fl/fl}$; *Osx*-GFP:Cre^{+} (*Gls1*$^{ob-}$) mice were considered as GLS1 conditional knockout mice in all experiments. As wild-type control, either Cre-negative littermates (i.e. *Gls1*$^{fl/fl}$; *Osx*-GFP:Cre^{-}; *Gls1*$^{ob+}$) or *Osx*-GFP:Cre^{+} (*Gls1*^{ctrl}) mice were used depending on the type of experiment. Briefly, for *in vivo* analyses *Gls1*$^{fl/fl}$; *Osx*-GFP:Cre^{-} mice were used, whereas for *ex vivo* (Western blot) and *in vitro* experiments, *Osx*-positive osteoprogenitors were isolated from 4-week-old *Osx*-GFP:Cre^{+} mice (Supplemental Figures 1A-C). Phenotypic analysis was performed on 8-week-old male mice unless otherwise mentioned. Mice (100% C57BL/6J background) were bred in conventional conditions in our animal housing facility (22°C to 24°C and 55% to 60% humidity in a room with a 12-hour light/dark cycle; Proefdierencentrum Leuven, Belgium), and were allowed unlimited access to water and regular rodent chow. Housing and experimental procedures were approved by the Institutional Animal Care and Research Advisory Committee of the KU Leuven.

Cell culture

This article is protected by copyright. All rights reserved.

Accepted Article

Cell isolation. *Osx*-positive cells were isolated based on GFP expression[25] by fluorescence-assisted cell sorting (FACS). Briefly, long bones were collected from 4-week-old male mice (1 week Dox withdrawal) and dissected from connective tissue and muscle. First, stromal cells from the periosteum were removed via collagenase-dispase digest (3 mg/ml collagenase and 4 mg/ml dispase in αMEM with glutaMAX-1 supplement, containing 100 units/ml penicillin and 50 µg/ml streptomycin; all from Gibco, Belgium) for one hour at 37°C under gentle agitation [26]. Next, epiphyses were cut away and bone marrow flushed out. The metaphyseal region of the bones was cut into small pieces and cells were isolated by incubating the fragments with a DNase I-liberase solution (DNase I 0.2mg/ml and liberase 0.2 mg/ml in αMEM with glutaMAX-1 supplement, containing 100 units/ml penicillin and 50 µg/ml streptomycin; all from Gibco) for 45 minutes at 37°C under gentle agitation. Isolated cells were passed through a 70 µm nylon mesh (BD Biosciences, USA) and hematopoietic cells were removed using the Lineage Cell Depletion Kit (Miltenyi Biotec, The Netherlands) according to the manufacturer's instructions. Finally, *Osx*-GFP positive cells were purified from the Lineage-depleted cell solution by FACS (BD FACSMelody, BD Biosciences) and seeded in growth medium (αMEM with glutaMAX-1 supplement, containing 100 units/ml penicillin, 50 µg/ml streptomycin and 10% fetal bovine serum (FBS); all from Gibco) for subsequent expansion. Passage 2-3 cells were used for all experiments. Periosteal cells were isolated from mouse long bones by enzymatic digest, as described by van Gastel *et al*. [26].

***Nutrient deprivation*.** FACS-sorted *Osx*-GFP positive cells were seeded in growth medium and after 24 hours washed with PBS and switched to control medium (αMEM with 100 units/ml penicillin, 50 µg/ml streptomycin, containing 5 mM glucose, 2.5 mM glutamine and 10% dialyzed FBS; all from Gibco), glucose deprivation medium (αMEM with 100 units/ml penicillin, 50 µg/ml streptomycin, containing 2.5 mM glutamine, different glucose concentrations (0 - 0.5 - 5 mM) and 10% dialyzed FBS), glutamine deprivation medium

This article is protected by copyright. All rights reserved.

Accepted Article

(αMEM with 100 units/ml penicillin, 50 µg/ml streptomycin, containing 5 mM glucose, different glutamine concentrations (0 - 0.025 - 0.25 - 2.5 mM) and 10% dialyzed FBS) or lipid-reduced serum (LRS) containing medium (αMEM with 100 units/ml penicillin, 50 µg/ml streptomycin, containing 5 mM glucose, 2.5 mM glutamine and 10% LRS). LRS was made by mixing FBS with fumed silica (Sigma-Aldrich) at 20 mg/ml for 3 hours at room temperature, followed by centrifugation at 2,000 g for 15 minutes and filtration of the supernatant through a 0.45 µm pore size filter [27].

***Osteogenic differentiation*.** For osteogenic differentiation, confluent *Osx*-GFP positive cells (expanded in full growth medium) were cultured in osteogenic differentiation medium, consisting of growth medium supplemented with 50 µg/ml ascorbic acid and 4 mM β-glycerophosphate (both Sigma-Aldrich). In certain experiments, full osteogenic differentiation medium containing all nutrients was switched to osteogenic deprivation medium (*i.e.* osteogenic differentiation medium with decreasing concentrations of glucose, glutamine or lipids; see above). Collagen deposition was analyzed after 3 days of osteogenic differentiation by picrosirius red staining. Briefly, cells were washed with PBS and fixed with 70% ethanol for one hour. After fixation, cells were washed with AD and stained with Sirius Red (0.17 M picric acid, 0.73 mM Direct Red 80 (Thermo Fisher Scientific, Belgium)) for one hour. Finally, cells were washed with 0.01 N HCl and air-dried. After 14 days of osteogenic differentiation, alkaline phosphatase staining was performed. Cells were washed with PBS and fixed with periodic acid lysin paraformaldehyde (75 mM lysine, 37.5 mM sodium phosphate buffer, 2% paraformaldehyde, 0.01 M $NaIO_4$) for 10 minutes. Cells were washed with AD and stained with Napthol AS-MX Fast Blue dye (0.269 mM Naphtol AS-MX, 0.5% N,N-dimethylformamid, 2 mM $MgCl_2$, 0.721 mM Fast Blue BB salt, 100 mM Tris-HCl) for one hour. Finally, stained cells were washed with AD and air-dried. Extracellular matrix mineralization was assessed after 21 days of differentiation using Alizarin red staining. Cells were washed with PBS and fixed with 100% methanol for 20 minutes at -20°C. After fixation,

This article is protected by copyright. All rights reserved.

the cells were rehydrated with AD for 5 minutes and stained with a 0.1% Alizarin Red solution for 30 minutes. Finally, stained cells were washed with AD and air-dried. All components were from Sigma-Aldrich unless otherwise specified.

In vitro treatments. In certain experiments, cells were treated with PTH (human PTH (1-34); Bachem AG, Switzerland), dimethyl-α-ketoglutarate (dimethyl-αKG, Sigma-Aldrich) or glutathione ethyl ester (GSH-EE, Sigma-Aldrich), or growth medium was supplemented with a 1x MEM Non-Essential Amino Acids (NEAAs) solution (Thermo Fisher Scientific) or a 1x EmbryoMax Nucleoside mixture (Merck, Belgium). PTH was dissolved in a sterile aqueous solution containing 0.9% NaCl, 0.1% BSA, 0.001 N HCl (also used as vehicle control), and used at 250 ng/mL for 48 hours unless otherwise indicated. Dimethyl-αKG was dissolved in DMSO and used at 0.5 mM; GSH-EE was solubilized in DMSO and used at 1mM. Treatment with dimethyl-αKG and GSH-EE, and supplementation with NEAA or nucleotides was for 72 hours.

Mass spectrometry

For isotopic labelling experiments, cells were incubated for 72 hours with $^{13}C_5$-glutamine (Cambridge Isotope Laboratories, USA) as described before [28,29]. Cells were rinsed with ice-cold 0.9% NaCl and metabolites for subsequent mass spectrometry analysis were prepared by scraping cells in 80% methanol supplemented with myristic acid. Phase separation was achieved by centrifugation at 4°C, and the methanol-water phase containing polar metabolites was separated and dried using a vacuum concentrator. Dried metabolite samples were stored at -80°C. To the dried fractions 25 µl of a 2% methoxyamine hydrochloride solution (20 mg dissolved in 1 ml pyridine) was added and incubated for 90 minutes at 37°C. Next, 75 µl of N-tert-Butyldimethylsilyl-N-methyltrifluoroacetamide with 1% N-tert-Butyldimethyl-chlorosilane (Sigma-Aldrich) was added for 30 minutes at 60°C. Reaction mixtures were centrifuged at 4°C for 15 minutes at 20,000 g in order to remove

Accepted Article

This article is protected by copyright. All rights reserved.

Accepted Article

insolubilities, the supernatant was transferred to a glass vial with conical insert (Agilent Technologies, Belgium). Separation of metabolites prior to mass spectrometry measurement was performed using a Dionex UltiMate 3000 LC System (Thermo Fisher Scientific) coupled to a Q Exactive Orbitrap mass spectrometer (Thermo Fisher Scientific) operating in negative ion mode. Practically, 15 µl of the extract was injected on a C18 column (Aquility UPLC®HSS T3 1.8 µm 2.1 × 100 mm) and the following gradient was performed by solvent A (H_2O, 10 mM Tributyl-Amine, 15 mM acetic acid) and solvent B (100% methanol). Chromatographic separation was achieved with a flowrate of 0.250 ml/min and the following gradient elution profile: 0 min, 0% B; 2 min, 0% B; 7 min, 37% B; 14 min, 41% B; 26 min, 100% B; 30 min, 100% B; 31 min, 0% B; 40 min, 0% B. The column was placed at 40 °C throughout the analysis. The mass spectrometer operated both in full scan mode (m/z range: 70-1050) using a spray voltage of 4.9 kV, capillary temperature of 320°C, sheath gas at 50.0, auxiliary gas at 10.0. The AGC target was set at 3e6 using a resolution of 140.000, with a maximum IT fill time of 512 ms. For data analysis, we used an in-house library, and metabolites of interest were analysed using Xcalibur software (Thermo Fisher Scientific). Total contribution of carbon was calculated using the following equation:

$$\text{total contribution of carbon} = \frac{\sum_{i=0}^{n} i * m_i}{\text{n} * \sum_{i=0}^{n} m_i}$$

where *n* is the number of C atoms in the metabolite, *i* represents the different mass isotopomers and *m* refers to the abundance of a certain mass. Isotope values were corrected for natural abundance using in-house developed software. For intracellular and extracellular metabolite levels, arbitrary units of the metabolites of interest were normalized to an internal standard and protein content. Glutamine uptake was calculated as the difference between glutamine levels in basal growth medium and spent medium. Energy charge was calculated as ([ATP] + ½ [ADP]) / ([ATP] + [ADP] + [AMP]).

RNA and protein expression analysis

This article is protected by copyright. All rights reserved.

Accepted Article

RNA expression. Total RNA from flushed femoral bone was extracted using the NucleoSpin RNA isolation kit (Machery Nagel, Germany) and mRNA was reverse transcribed using Superscript II Reverse Transcriptase (Thermo Fisher Scientific). qRT-PCR was performed on the 7500 Fast Real-Time PCR System (Applied Biosystems, Belgium) using specific forward and reverse oligonucleotide primers (Supplemental Table 1). Expression levels were analysed using the $2^{-\Delta\Delta Ct}$ method and were normalized for *Hprt* expression.

Protein expression. Total cell lysates from cultured cells were obtained after cell lysis in 62.5 mM Tris buffer (pH 6.8) containing 10% glycerol, 2% SDS, 1x cOmplete proteinase inhibitor cocktail (Roche, Belgium) and 1x PhosSTOP phosphatase inhibitor cocktail (Roche). For protein extraction from metaphyseal bone, long bones were isolated and cleaned of excess muscle. Epiphyses were cut and bone marrow was flushed using PBS. Bones were then snap-frozen in liquid nitrogen and crushed in 62.5 mM Tris buffer (pH 6.8) containing 10% glycerol, 2% SDS, 1x cOmplete proteinase inhibitor cocktail (Roche) and 1x PhosSTOP phosphatase inhibitor cocktail (Roche). Protein concentration was determined with the BCA Protein Assay Reagent (Thermo Fisher Scientific). Proteins were separated by SDS-PAGE under reducing conditions and transferred to a nitrocellulose membrane (GE Healthcare, Belgium). Membranes were blocked with 5% dry milk or bovine serum albumin (Sigma-Aldrich) in TBS with 0.1% Tween-20 for 30 minutes at room temperature and incubated overnight at 4°C with primary antibodies against AMPK (rabbit, 1:1000 dilution; #2532, Cell Signaling Technologies, USA), p-AMPK^{T172} (rabbit, 1:1000 dilution; #2535, Cell Signaling Technologies), β-actin (mouse, 1:2500 dilution; A5441, Sigma-Aldrich), GLS1 (rabbit, 1:1000 dilution; ab93434, Abcam, UK), or SLC1A5 (rabbit, 1:1000 dilution; #8057, Cell Signaling Technology). Signals were detected by enhanced chemiluminescence (PerkinElmer, Belgium) after incubation with appropriate HRP-conjugated secondary antibodies. For (p-)AMPK, GLS1 and SLC1A5 a goat-anti-rabbit secondary antibody (1:2500 dilution; P0448, Dako) was used, whereas β-actin expression was detected using a rabbit-anti-mouse (1:2500; P0161, Dako) secondary antibody.

This article is protected by copyright. All rights reserved.

Accepted Article

Proliferation analysis

Proliferation was measured by 5'-bromo-2'-deoxyuridine (BrdU) incorporation, added during the last 4 hours of culture, and detected using the Cell Proliferation Biotrack ELISA system (GE Healthcare), and values were normalized to the amount of DNA.

Flow cytometry

Protein synthesis. Protein synthesis was analyzed using the Click-iT® L-homopropargylglycine (HPG) Alexa Fluor® 594 Protein Synthesis Assay Kit (Thermo Fisher Scientific) according to the manufacturer's instructions. Briefly, adherent osteoprogenitors were incubated with 50 µM Click-iT® HPG overnight in growth medium. Cells were then trypsinized and fixed with 3.7% formaldehyde for 15 minutes at room temperature, washed and permeabilized with 0.5% Triton X-100 for 20 minutes at room temperature. Subsequently, cells were incubated with Click-iT® reaction cocktail for 30 minutes at room temperature protected from light, washed and fluorescence was detected by flow cytometry. Data were analyzed using Kaluza software (Beckman Coulter, Belgium) and plotted as mean fluorescence intensity.

Cell viability. Cell death of cultured osteoprogenitors was detected by flow cytometry using Annexin V-APC and propidium iodide (PI) (Dead Cell Apoptosis Kit; Thermo Fisher Scientific) as described before [28], where Annexin V^- PI^- cells were considered viable. Data were analyzed using Kaluza software.

Reactive Oxygen Species (ROS) Levels. Intracellular ROS levels were detected by the use of a fluorescent probe dye, CellROX Deep Red (Thermo Fisher Scientific). Cells were incubated with 10 µM CellROX for 30 minutes at 37°C, and fluorescence was detected by flow cytometry. Data were analyzed using Kaluza software and plotted as mean fluorescence intensity.

This article is protected by copyright. All rights reserved.

Accepted Article

Collagen synthesis

Collagen synthesis was quantified *in vitro* by incubation of cultured *Osx*-GFP positive cells with 20 µCi/ml ^{3}H-proline (PerkinElmer) as described before [29]. After overnight labeling, cells were lysed in extraction buffer (11% acetic acid H_2O with 0.25% bovine serum albumin) and proteins were precipitated by the addition of 20% trichloroacetic acid. Radioactivity was determined by liquid scintillation counting, and normalized for DNA content.

***In vivo* PTH treatment**

Eight-week-old male mice were injected with either 80 µg/kg PTH (human PTH (1-34), Bachem AG) or vehicle control (0.9% NaCl solution containing 0.1% bovine serum albumin and 0.001 N HCl) 5 days per week for 4 weeks. Three days after the final PTH injection, tibiae and serum were collected for subsequent analysis, and metaphyseal bone protein extracts were prepared as described above.

X-ray microtomography (microCT)

MicroCT analysis of mineralized bone mass was performed using a desktop micro-tomographic image system and related software, as described before [29,30]. Briefly, tibias were scanned using the SkyScan 1172 microCT system (Bruker, Belgium) at a pixel size of 5 µm with 50 kV tube voltage, 200 µA current and 0.5 mm aluminum filter. Projection data was reconstructed using the NRecon software (Bruker), trabecular and cortical volumes of interest were selected manually (for trabecular the region between 0.5 to 3.5 mm distal from the growth plate and cortical between 2 and 2.5 mm) and 3D morphometric parameters were calculated using CT Analyzer software (Bruker) at a threshold index of 100 to 255 (global Otsu thresholding). Data were shown according to the guidelines of the American Society for Bone and Mineral Research [31]. 3D image rendering was performed using 3D-Visualization software (Bruker).

This article is protected by copyright. All rights reserved.

Accepted Article

Serum biochemistry

Serum osteocalcin was measured by an in-house radioimmunoassay [30] and serum CTx-I levels were measured by a RatLaps ELISA kit (Immunodiagnostic Systems, UK).

Histochemistry and histomorphometry

Histomorphometric analysis of murine tibiae was performed as previously described [29,30,32]. Briefly, osteoblasts were quantified on H&E-stained sections, and osteoclasts were visualized on TRAP-stained sections. Unmineralized (osteoid) and mineralized bone matrix was quantified on Goldner or Von Kossa-stained sections, respectively. To analyze dynamic bone parameters, calcein (16 mg/kg body weight; Sigma-Aldrich) was administered via intraperitoneal injection 4 days and 1 day prior to sacrifice.

Images were acquired on an Axioplan 2 microscope (Zeiss, Belgium) and histomorphometric analyses were performed using related Axiovision software (Zeiss). Measurements were performed on three sections, each at least 40 µm apart. For each section, three consecutive regions of interest were quantified along the vertical axis of the central metaphysis, starting at 150 µm from the distal end of the growth plate. The total area per section considered for histomorphometry was 1800 mm^2. Data were expressed according to the American Society for Bone and Mineral Research standardized histomorphometry nomenclature [33].

Statistics

Data are presented as means ± SD. *n* values represent the number of independent experiments performed or the number of individual mice phenotyped. For each independent *in vitro* experiment, at least three technical replicates were used. For immunoblots, representative images were shown of at least three independent experiments using samples from different cell lysates. Investigators were blinded during animal handling and (*in vitro*/*in vivo*) endpoint measurements. For the *in vivo* PTH treatment experiments, mice were randomly assigned to experimental groups. Data were analyzed by two-sided two-sample

This article is protected by copyright. All rights reserved.

Student's *t*-test, and two-way ANOVA with Tukey-Kramer post-hoc test using the NCSS statistical software. Differences were considered statistically significant at $p<0.05$.

Accepted Article

This article is protected by copyright. All rights reserved.

Accepted Article

Results

Glutamine is a critical nutrient for osteoprogenitor function

To examine the nutritional requirements of osteoprogenitor function *in vitro*, we isolated *Osx*-positive cells from the metaphyseal bone of 4-week-old *Osx*-GFP:Cre^{+} transgenic mice by fluorescence-assisted cell sorting (FACS) (Figure 1A). In accordance with reported findings [15,16,27], deprivation of exogenous glucose or lipids significantly impaired osteoprogenitor function *in vitro*, evidenced by decreased proliferation and survival, as shown by BrdU incorporation and Annexin V - PI flow cytometry, respectively (Supplemental Figures 2A,B). Moreover, osteogenic differentiation capacity was reduced, evidenced by picrosirius red (i.e. collagen deposition), alkaline phosphatase (i.e. early differentiation) and alizarin red (i.e. late differentiation/mineralization) staining (Supplemental Figure 2C). In addition, withdrawal of glutamine from the culture media similarly impaired osteoprogenitor proliferation, survival and differentiation into the osteoblast lineage (Figures 1B-D), indicating that glutamine is a necessary nutrient for normal osteoprogenitor function.

Osteoprogenitor-specific GLS1 deletion decreases bone mass

To characterize the functional role of glutamine metabolism in osteoprogenitors *in vivo*, we deleted the rate-limiting enzyme GLS1 by crossing *Gls1*$^{fl/fl}$ mice with *Osx*-GFP:Cre transgenic mice. *Gls1*$^{fl/fl}$; *Osx*-GFP:Cre^{-} (*Gls1*$^{ob+}$; wild-type) and *Gls1*$^{fl/fl}$; *Osx*-GFP:Cre^{+} (*Gls1*$^{ob-}$; conditional knockout) mice were maintained on doxycycline (Dox) from conception until 3 weeks of age before withdrawing Dox for 5 weeks (Figure 2A). Of note, to analyze *ex vivo* or *in vitro* the effect of GLS1 inactivation specifically in osteoprogenitor cells, *Osx*-positive cells were isolated from *Osx*-GFP:Cre^{+} (*Gls1*^{ctrl}) and *Gls1*$^{ob-}$ mice treated according to the same Dox regimen. *Gls1*^{ctrl} mice were used as wild-type control for these experiments since GFP expression, necessary for FACS sorting, occurs together with Cre recombinase expression [25]. Dox withdrawal resulted in specific and efficient GLS1 inactivation in *Osx*-positive cells and their progeny (Figure 2B and Supplemental Figure 3A). *Gls1*$^{ob-}$ mice did not display any

This article is protected by copyright. All rights reserved.

Accepted Article

changes in body weight or tibia length (Supplemental Figures 3B,C), but showed significantly decreased bone mass at 8 weeks of age, as evidenced by *ex vivo* micro-computed tomography (Figures 2C-E). Trabecular bone volume was reduced by almost 60%, which was caused by a decrease in trabecular number and thickness, resulting in an increase in trabecular separation (Supplemental Figures 3D-F). Moreover, cortical thickness was decreased by 15% in *Gls1*$^{ob-}$ mice, which was related to a decrease in periosteal perimeter and an increase in endocortical perimeter together with a reduction in medullary area (Figure 2E and Supplemental Figures 3G-I). Cortical porosity was not affected in mutant mice (Supplemental Figure 3J). Of note, *Gls1*^{ctrl} and *Gls1*$^{ob+}$ mice were indistinguishable in trabecular and cortical bone parameters (Supplemental Figures 3K,L), thereby validating their use as control animals. Taken together, GLS1-mediated glutamine catabolism in osteoprogenitors is required for postnatal bone accrual.

Bone formation is impaired in *Gls1*$^{ob-}$ mice

Based on our *in vitro* findings that osteoblasts depend on glutamine for their function, we reasoned that bone formation was impaired in *Gls1*$^{ob-}$ mice. Histomorphometry of H&E-stained sections revealed a decrease in the number and surface of cuboidal osteoblasts lining the bone trabeculae (Figures 2F,G and Supplemental Figure 3M). Moreover, we observed reduced osteoblast activity in *Gls1*$^{ob-}$ mice, evidenced by a decrease in osteoid thickness and surface (Supplemental Figures 3N-P), and in its subsequent mineralization (Figures 2H-J), as analyzed by Goldner staining and *in vivo* calcein labeling, respectively. Consistently, serum osteocalcin levels and femoral transcripts of osteoblast markers including collagen type I (*Col1*) and osteocalcin (*Ocn*) were decreased in *Gls1*$^{ob-}$ mice (Figure 2K and Supplemental Figure 3Q). Of note, the expression of runt-related transcription factor 2 (*Runx2*) was not altered in mutant mice, likely because this transcription factor functions upstream of Osterix [9]. In contrast to the profound reduction in bone formation parameters, GLS1 deletion in osteoprogenitors did not affect bone resorption, as we observed no quantitative changes in TRAP-stained osteoclasts per bone surface and serum CTx-I levels

This article is protected by copyright. All rights reserved.

Accepted Article

(Figures 2L-N). Thus, glutamine metabolism, through GLS1, is required for osteoblast function during bone mass accrual.

GLS1 deletion impairs osteoprogenitor anabolism and viability

We next determined how GLS1 deletion impairs osteoprogenitor function, by isolating *Osx*-GFP positive cells from the bone metaphysis of 4-week-old *Gls1*^{ctrl} and *Gls1*$^{ob-}$ mice by FACS (Figure 3A). After sorting, we obtained fewer GFP-positive osteoprogenitors from *Gls1*$^{ob-}$ mice (Supplemental Figures 4A-C), which is in line with the reduced osteoblast number quantified by histomorphometry. After plating, isolated osteoprogenitors from *Gls1*$^{ob-}$ mice displayed a significant reduction in proliferation and cell survival, which was associated with increased intracellular ROS levels (Figures 3B-D). Moreover, when cultured in media containing osteogenic stimuli, mutant cells showed decreased osteogenic differentiation (Figure 3E). Interestingly, the differentiation defect was already prominent after 3 days of culture, suggesting that GLS1 deletion impairs matrix deposition, which in turn delays proper osteogenic differentiation and mineralization.

Proliferation, survival and matrix production during osteogenic differentiation are closely intertwined with cellular metabolic fitness [15-17]. To provide a link between glutamine metabolism and osteoprogenitor function, we first used stable isotopically labeled glutamine to trace the metabolic fate of glutamine in different pathways. Briefly, sorted *Osx*-GFP positive cells were cultured in the presence of $^{13}C_5$-glutamine for 3 days and the contribution of glutamine-derived carbon to downstream metabolites was determined by measuring the mass isotope-labeling pattern (Figure 3F). As expected, in control cells, a significant amount of glutamate was derived from glutamine, and glutamine carbon contributed to TCA cycle intermediates, amino acids such as aspartate and proline, nucleotides and the antioxidant glutathione (Figures 3G-P). Importantly, glutamine not only labeled TCA cycle intermediates and their derivates via oxidation (e.g. citrate m+4, fumarate/malate/aspartate m+4), but also through reductive carboxylation, although to a lesser degree (e.g. citrate m+5,

This article is protected by copyright. All rights reserved.

Accepted Article

fumarate/malate/aspartate m+3) (Figures 3J-M). Deletion of GLS1 impaired glutamine contribution to TCA cycle intermediates (both through oxidation and reductive carboxylation), amino acids, nucleotides and glutathione (Figures 3G-P), resulting in a significant reduction of their intracellular levels (Figure 3Q). Taken together, these data suggest that GLS1-mediated glutamine catabolism supports anabolic processes and redox homeostasis in osteoprogenitors.

Next, we aimed to prove the link between the decrease in anabolic and redox precursor metabolites with impaired osteoprogenitor function upon GLS1 deletion by rescue experiments. First, we focused on proliferation and supplemented *Osx*-GFP positive cells with a nucleoside mixture or non-essential amino acids (NEAA). Whereas nucleosides or NEAA alone did not affect cell proliferation, combined administration fully rescued the proliferation defect in GLS1 null cells (Figure 4A). Second, osteogenic differentiation capacity of GLS1-deficient cells was also restored by supplementation of NEAA (Figure 4B). Mechanistically, NEAA treatment completely restored total protein and collagen synthesis, resulting in normalized matrix deposition evidenced by picrosirius red staining, that supported osteogenic differentiation (Figures 4B-D). Third, the combined effects on proliferation, protein and matrix synthesis, and osteogenic differentiation were rescued by supplementation with αKG, an anaplerotic precursor metabolite, as this strategy restored the levels of TCA cycle intermediates and amino acids (Figures 4E-I). Importantly, the defect in biosynthesis was not related to changes in energy homeostasis, since deletion of GLS1 did not affect ATP levels, energy charge or AMPK signaling (Supplemental Figures 5A-C). Together, GLS1 is necessary for osteoprogenitor proliferation and differentiation through nucleotide and NEAA synthesis.

Normalizing biosynthesis in GLS1-deficient osteoprogenitors restored proliferation and differentiation, but it did not rescue the defect in redox homeostasis and cell survival, likely because GSH levels were still low (Figure 4E and Supplemental Figures 6A,B). To prove the

This article is protected by copyright. All rights reserved.

Accepted Article

contribution of reduced GSH levels to impaired redox balance and viability, we treated osteoprogenitors with a cell-permeable glutathione ethyl ester (GSH-EE). This approach prevented ROS accumulation in control cells and GLS1 null cells, and rescued the decrease in cell survival (Figures 4J,K), indicating that GLS1-mediated glutamine catabolism in osteoprogenitors is necessary for maintaining adequate redox homeostasis. During differentiation, GSH-EE supplementation only minimally restored matrix deposition and mineralization by GLS1-deficient cells (Supplemental Fig. 6C), suggesting that their impaired osteogenic differentiation capacity is primarily caused by a defect in biosynthesis.

PTH stimulates glutamine uptake and GLS1-mediated catabolism in osteoprogenitors

Given the important contribution of GLS1 to osteoprogenitor function, we questioned whether glutamine metabolism is also involved in the osteoanabolic effect of PTH treatment. First, we determined the expression of key glutamine transporters and pathway enzymes in FACS-sorted *Osx*-positive cells after incubation with PTH for 48 hours at different concentrations (Figure 5A). PTH at 50 ng/ml did not have an effect, but at 100ng/ml it increased the expression of the glutamine transporters *Slc1a5*, *Slc38a1*, and *Slc38a3*, as well as *Gls1* and *glutamate dehydrogenase 1* with a maximal response at 250 ng/ml (Figure 5B). In line, SLC1A5 and GLS1 protein levels were significantly increased after 48 hours treatment with 250 ng/ml PTH (Figure 5C), suggesting that PTH activates glutamine metabolism in osteoprogenitors.

The PTH-induced molecular changes in glutamine metabolism prompted us to examine the effect of PTH on the metabolic fate of glutamine. In accordance with the increased expression of glutamine transporters, PTH treatment at 250 ng/ml enhanced uptake of glutamine (Figure 5D), which was subsequently more catabolized in downstream pathways. Indeed, using ^{13}C-glutamine tracing, we found that PTH treatment increased glutamine carbon incorporation in TCA cycle intermediates, amino acids and glutathione, resulting in increased intracellular levels, whereas glutamine contribution to UMP was not altered

This article is protected by copyright. All rights reserved.

Accepted Article

(Figures 5E-O). Of note, the enhanced glutamine labeling in TCA cycle intermediates and downstream metabolites was through glutamine oxidation rather than reductive carboxylation (Figures 5H-K).

Finally, to prove the contribution of GLS1 in PTH-induced flux of glutamine to anabolic and redox pathways, we treated FACS-sorted *Osx*-positive GLS1 null cells with PTH at 250 ng/ml for 48 hours (Figure 6A). Whereas the PTH-mediated increase in glutamine uptake was still present in GLS1-deficient osteoprogenitors, the intracellular levels of TCA cycle intermediates, amino acids and glutathione were significantly decreased (Figures 6B,C), indicating that glutamine flux in downstream pathways was impaired.

Taken together, PTH treatment of osteoprogenitors stimulates glutamine uptake and GLS1-mediated flux in anabolic and redox pathways *in vitro*.

GLS1-mediated glutamine catabolism contributes to PTH-induced bone anabolism

Based on our *in vitro* PTH findings, we questioned whether the adaptations in glutamine metabolism contribute to the anabolic bone response induced by intermittent PTH administration. As a model, we treated 8-week-old *Gls1*$^{ob+}$ and *Gls1*$^{ob-}$ mice 5 times a week with PTH for 4 weeks (Figure 7A). Of note, mice were kept on Dox until 8 weeks of age, which avoided a baseline bone phenotype caused by GLS1 deletion (Supplemental Figures 7A,B). We first evaluated whether PTH elicited similar changes in glutamine metabolism as observed *in vitro*. PTH administration enhanced the expression of SLC1A5 in metaphyseal bone protein extracts of both genotypes, whereas GLS1 levels were only increased in *Gls1*$^{ob+}$ mice (Figure 7B). Moreover, PTH treatment increased trabecular bone volume in *Gls1*$^{ob+}$ mice, but this effect was not observed in *Gls1*$^{ob-}$ mice (Figures 7C,D and Supplemental Figures 8A-C). Of note, the anabolic effect of PTH on cortical bone was not statistically significant in any of the genotypes (Supplemental Figure 8D). Thus, GLS1-mediated

This article is protected by copyright. All rights reserved.

glutamine metabolism in osteoprogenitors is required for the PTH-induced bone anabolic effect.

We finally investigated the cellular basis of the lack of a bone anabolic response in PTH-treated *Gls1*$^{ob-}$ mice. Histomorphometric analysis of H&E-stained sections revealed that GLS1 deletion in *Osx*-positive cells attenuated the increase in osteoblast number caused by PTH (Figures 7E,F and Supplemental Figure 8E). Moreover, the PTH-induced increase in osteoblast activity was completely blunted in *Gls1*$^{ob-}$ mice, as evidenced by histomorphometry and serum osteocalcin levels (Figures 7G-L and Supplemental Figure 8F). On the other hand, GLS1 inactivation did not alter osteoclast number or activity in PTH-treated *Gls1*$^{ob+}$ or *Gls1*$^{ob-}$ mice (Supplemental Figures 8G-I). Taken together, GLS1-mediated glutamine catabolism is necessary for the PTH-dependent increase in osteoblast number and activity *in vivo*.

Accepted Article

This article is protected by copyright. All rights reserved.

Accepted Article

Discussion

The anabolic functions of osteolineage cells are critical to acquire and preserve bone mass, but their nutritional requirements are not fully understood. In this study we show that glutamine metabolism in osteoprogenitors is a key regulator of postnatal bone mass accrual and of the PTH-induced osteo-anabolic response. Deletion of GLS1 results in an osteopenic bone phenotype by impairing bone formation. Mechanistically, GLS1-mediated glutamine catabolism controls osteoprogenitor function through a dual mechanism: glutamine-derived nucleotides and amino acids are critical for biosynthesis, whereas glutamine-mediated GSH synthesis is necessary for proper redox homeostasis and cell survival.

Skeletal progenitor cells proliferate prior to differentiation into extracellular matrix-synthesizing osteoblasts [8,9]. However, the metabolic regulation of these processes is incompletely understood. In general, proliferation and matrix synthesis heavily rely on amino acids that are used for biomass production [34]. Not surprisingly, glutamine, the most abundant circulating amino acid [18], is a critical carbon and nitrogen donor to sustain these anabolic processes in many (non-)malignant cell types [19-21,35]. In this study, using isotopic labeling and metabolic rescue experiments, we show that GLS1-mediated glutamine catabolism is required for osteoprogenitor biosynthesis through generation of nucleotides and amino acids. Importantly, GLS1-deficient cells were not in energy deficit, indicating that other nutrients such as glucose or fatty acids could compensate or are more used for ATP synthesis [15,16]. These findings are in line with our recent study in growth plate chondrocytes, showing a similar glutamine dependence for proper functioning [36], although two differences are noted. First, the rate of glutamine metabolism differs, as glutamine uptake and GLS1-mediated flux to TCA cycle intermediates and amino acids is higher in chondrocytes compared to skeletal progenitors [36]. A plausible explanation is the avascular microenvironment wherein chondrocytes reside [10], making them dependent on nutrient diffusion, which is especially low for fatty acids. Accordingly, chondrocytes show a low

This article is protected by copyright. All rights reserved.

Accepted Article

uptake and oxidation of fatty acids, in contrast to osteoprogenitors which function in close vicinity of blood vessels [13,27]. Thus, chondrocytes rely more on carbon from other nutrients like glutamine for TCA cycle anaplerosis, explaining the higher rate of glutamine metabolism compared to osteoprogenitors. A second difference is that glutamine metabolism in chondrocytes also regulates chondrogenic gene expression by epigenetic changes [36], a feature not observed in osteoprogenitors. Together, these data indicate that different skeletal cell types allocate glutamine-derived carbons to specific metabolic fates to support their cellular function.

Extensive studies have indicated that PTH stimulates bone formation through, amongst other mechanisms, enhanced osteoblast activity [37]. We now demonstrate that PTH stimulates GLS1-mediated catabolism likely to sustain the increased extracellular matrix production, evidenced by the enhanced production of amino acids for protein synthesis. PTH also increases glycolysis in the MC3T3 osteoblastic cell line at the expense of glucose oxidation [38]. However, oxidative phosphorylation is still increased by PTH [38], arguing that other nutrients like glutamine or fatty acids might be used for energy generation [16,39]. Based on our data, we speculate that glutamine is likely not involved, given the lack of an energy deficit upon GLS1 inactivation. How PTH induces glutamine uptake and catabolism remains to be fully elucidated. Possibly, PTH converges with other growth-related signaling factors like c-MYC or mammalian target of rapamycin (mTOR) to directly or indirectly regulate glutamine metabolism [36,38,40-42]. Regardless of the mechanism, the PTH-induced stimulation of glutamine metabolism is physiologically relevant since PTH increases the expression of the glutamine transporter SLC1A5 and GLS1 in *Osx*-positive cells *in vivo*, and GLS1 deletion fully blunts the osteoanabolic response.

In addition to maintaining biosynthesis, osteolineage cells require a stringent control of redox homeostasis to keep ROS levels in check and to avoid oxidative stress [43,44]. In line with our previous studies [28,36], we demonstrate that glutamine serves as a precursor metabolite for

This article is protected by copyright. All rights reserved.

de novo GSH synthesis in *Osx*-positive cells to maintain redox balance and cell viability. Interestingly, PTH treatment enhances glutamine carbon flux to glutathione and increases GSH levels, suggesting that this metabolic reprogramming contributes to the anti-oxidant features of PTH [45]. Whether and how other nutrients contribute to glutathione synthesis and redox homeostasis in osteogenic cells remains unknown and requires further study.

Taken together, our findings provide new insights into the nutritional regulation of osteoprogenitor function. We propose that glutamine, through GLS1-mediated catabolism, is necessary for osteoblast biosynthesis and redox homeostasis, and thereby controls postnatal bone mass accrual. In addition, glutamine metabolism is required to enable the osteoanabolic response to PTH administration. A limitation is that we only used young adult male mice for this study. Yet, our data clearly indicate that the metabolic profile of osteoprogenitors regulates their function *in vivo*, suggesting that metabolic modulation of skeletal cells might be an interesting strategy to improve bone anabolism in osteoporotic patients, although this hypothesis warrants further investigation.

Accepted Article

This article is protected by copyright. All rights reserved.

Acknowledgments

The authors wish to thank I. Stockmans and K. Moermans for technical assistance. G.C. acknowledges funding from Fund for Scientific Research-Flanders (FWO: G.0964.14, G.0A42.16 and G.0B3418) and from KU Leuven (C24/17/077); P.C. from long-term structural funding – Methusalem Funding by the Flemish Government and ERC Advanced Research Grant (EU-ERC743074). S.S. is a postdoctoral fellow from the FWO (12H5917N), C.-S. D. received funding from Marie Skłodowska-Curie actions (841199 - META2 - H2020-MSCA-IF-2018 H2020). The authors declare no conflict of interest.

Author Contributions

Conceptualization: S.S. and G.C.; Investigation: S.S., C.-S. D., S.T., R.V.L.; Resources: P.C.; Funding Acquisition: S.S. and G.C.; Writing - Original Draft: S.S. and G.C.; Supervision: G.C.

Accepted Article

This article is protected by copyright. All rights reserved.

Accepted Article

References

1. Sims NA, Martin TJ. Coupling the activities of bone formation and resorption: a multitude of signals within the basic multicellular unit. Bonekey Rep. Jan 8 2014;3:481. Epub 2014/01/28.

2. Hendrickx G, Boudin E, Van Hul W. A look behind the scenes: the risk and pathogenesis of primary osteoporosis. Nat Rev Rheumatol. Aug 2015;11(8):462-74. Epub 2015/04/23.

3. Park D, Spencer JA, Koh BI, Kobayashi T, Fujisaki J, Clemens TL, et al. Endogenous bone marrow MSCs are dynamic, fate-restricted participants in bone maintenance and regeneration. Cell Stem Cell. Mar 2 2012;10(3):259-72. Epub 2012/03/06.

4. Mizoguchi T, Pinho S, Ahmed J, Kunisaki Y, Hanoun M, Mendelson A, et al. Osterix marks distinct waves of primitive and definitive stromal progenitors during bone marrow development. Dev Cell. May 12 2014;29(3):340-9. Epub 2014/05/16.

5. Kiernan J, Davies JE, Stanford WL. Concise Review: Musculoskeletal Stem Cells to Treat Age-Related Osteoporosis. Stem Cells Transl Med. Oct 2017;6(10):1930-9. Epub 2017/08/24.

6. Minisola S, Cipriani C, Grotta GD, Colangelo L, Occhiuto M, Biondi P, et al. Update on the safety and efficacy of teriparatide in the treatment of osteoporosis. Ther Adv Musculoskelet Dis. 2019;11:1759720X19877994. Epub 2019/10/22.

7. Bovijn J, Krebs K, Chen CY, Boxall R, Censin JC, Ferreira T, et al. Evaluating the cardiovascular safety of sclerostin inhibition using evidence from meta-analysis of clinical trials and human genetics. Sci Transl Med. Jun 24 2020;12(549). Epub 2020/06/26.

8. Harada S, Rodan GA. Control of osteoblast function and regulation of bone mass. Nature. May 15 2003;423(6937):349-55. Epub 2003/05/16.

9. Long F. Building strong bones: molecular regulation of the osteoblast lineage. Nat Rev Mol Cell Biol. Dec 22 2011;13(1):27-38. Epub 2011/12/23.

This article is protected by copyright. All rights reserved.

Accepted Article

10. Stegen S, Carmeliet G. Hypoxia, hypoxia-inducible transcription factors and oxygen-sensing prolyl hydroxylases in bone development and homeostasis. Curr Opin Nephrol Hypertens. Jul 2019;28(4):328-35. Epub 2019/04/16.

11. Schieber M, Chandel NS. ROS function in redox signaling and oxidative stress. Curr Biol. May 19 2014;24(10):R453-62. Epub 2014/05/23.

12. Zoch ML, Abou DS, Clemens TL, Thorek DL, Riddle RC. In vivo radiometric analysis of glucose uptake and distribution in mouse bone. Bone Res. 2016;4:16004. Epub 2016/04/19.

13. Kim SP, Li Z, Zoch ML, Frey JL, Bowman CE, Kushwaha P, et al. Fatty acid oxidation by the osteoblast is required for normal bone acquisition in a sex- and diet-dependent manner. JCI Insight. Aug 17 2017;2(16). Epub 2017/08/18.

14. Lee WC, Guntur AR, Long F, Rosen CJ. Energy Metabolism of the Osteoblast: Implications for Osteoporosis. Endocr Rev. Jun 1 2017;38(3):255-66. Epub 2017/05/05.

15. Karner CM, Long F. Glucose metabolism in bone. Bone. Oct 2018;115:2-7. Epub 2017/08/28.

16. Kushwaha P, Wolfgang MJ, Riddle RC. Fatty acid metabolism by the osteoblast. Bone. Oct 2018;115:8-14. Epub 2017/09/03.

17. Dirckx N, Moorer MC, Clemens TL, Riddle RC. The role of osteoblasts in energy homeostasis. Nat Rev Endocrinol. Nov 2019;15(11):651-65. Epub 2019/08/30.

18. Walsh NP, Blannin AK, Robson PJ, Gleeson M. Glutamine, exercise and immune function. Links and possible mechanisms. Sports Med. Sep 1998;26(3):177-91. Epub 1998/11/05.

19. DeBerardinis RJ, Cheng T. Q's next: the diverse functions of glutamine in metabolism, cell biology and cancer. Oncogene. Jan 21 2010;29(3):313-24. Epub 2009/11/03.

20. Altman BJ, Stine ZE, Dang CV. From Krebs to clinic: glutamine metabolism to cancer therapy. Nat Rev Cancer. Oct 2016;16(10):619-34. Epub 2016/08/06.

This article is protected by copyright. All rights reserved.

Accepted Article

21. Zhang J, Pavlova NN, Thompson CB. Cancer cell metabolism: the essential role of the nonessential amino acid, glutamine. EMBO J. May 15 2017;36(10):1302-15. Epub 2017/04/20.

22. Yu Y, Newman H, Shen L, Sharma D, Hu G, Mirando AJ, et al. Glutamine Metabolism Regulates Proliferation and Lineage Allocation in Skeletal Stem Cells. Cell Metab. Apr 2 2019;29(4):966-78 e4. Epub 2019/02/19.

23. Karner CM, Esen E, Okunade AL, Patterson BW, Long F. Increased glutamine catabolism mediates bone anabolism in response to WNT signaling. J Clin Invest. Feb 2015;125(2):551-62. Epub 2015/01/07.

24. Mingote S, Masson J, Gellman C, Thomsen GM, Lin CS, Merker RJ, et al. Genetic Pharmacotherapy as an Early CNS Drug Development Strategy: Testing Glutaminase Inhibition for Schizophrenia Treatment in Adult Mice. Front Syst Neurosci. 2015;9:165. Epub 2016/01/19.

25. Rodda SJ, McMahon AP. Distinct roles for Hedgehog and canonical Wnt signaling in specification, differentiation and maintenance of osteoblast progenitors. Development. Aug 2006;133(16):3231-44. Epub 2006/07/21.

26. van Gastel N, Torrekens S, Roberts SJ, Moermans K, Schrooten J, Carmeliet P, et al. Engineering vascularized bone: osteogenic and proangiogenic potential of murine periosteal cells. Stem Cells. Nov 2012;30(11):2460-71. Epub 2012/08/23.

27. van Gastel N, Stegen S, Eelen G, Schoors S, Carlier A, Daniels VW, et al. Lipid availability determines fate of skeletal progenitor cells via SOX9. Nature. Mar 2020;579(7797):111-7. Epub 2020/02/28.

28. Stegen S, van Gastel N, Eelen G, Ghesquiere B, D'Anna F, Thienpont B, et al. HIF-1alpha Promotes Glutamine-Mediated Redox Homeostasis and Glycogen-Dependent Bioenergetics to Support Postimplantation Bone Cell Survival. Cell Metab. Feb 9 2016;23(2):265-79. Epub 2016/02/11.

This article is protected by copyright. All rights reserved.

Accepted Article

29. Stegen S, Laperre K, Eelen G, Rinaldi G, Fraisl P, Torrekens S, et al. HIF-1alpha metabolically controls collagen synthesis and modification in chondrocytes. Nature. Jan 2019;565(7740):511-5. Epub 2019/01/18.

30. Stegen S, Stockmans I, Moermans K, Thienpont B, Maxwell PH, Carmeliet P, et al. Osteocytic oxygen sensing controls bone mass through epigenetic regulation of sclerostin. Nat Commun. Jul 2 2018;9(1):2557. Epub 2018/07/04.

31. Bouxsein ML, Boyd SK, Christiansen BA, Guldberg RE, Jepsen KJ, Muller R. Guidelines for assessment of bone microstructure in rodents using micro-computed tomography. J Bone Miner Res. Jul 2010;25(7):1468-86. Epub 2010/06/10.

32. Tournaire G, Stegen S, Giacomini G, Stockmans I, Moermans K, Carmeliet G, et al. Nestin-GFP transgene labels skeletal progenitors in the periosteum. Bone. Apr 2020;133:115259. Epub 2020/02/10.

33. Dempster DW, Compston JE, Drezner MK, Glorieux FH, Kanis JA, Malluche H, et al. Standardized nomenclature, symbols, and units for bone histomorphometry: a 2012 update of the report of the ASBMR Histomorphometry Nomenclature Committee. J Bone Miner Res. Jan 2013;28(1):2-17. Epub 2012/12/01.

34. Hosios AM, Hecht VC, Danai LV, Johnson MO, Rathmell JC, Steinhauser ML, et al. Amino Acids Rather than Glucose Account for the Majority of Cell Mass in Proliferating Mammalian Cells. Dev Cell. Mar 7 2016;36(5):540-9. Epub 2016/03/10.

35. Li X, Sun X, Carmeliet P. Hallmarks of Endothelial Cell Metabolism in Health and Disease. Cell Metab. Sep 3 2019;30(3):414-33. Epub 2019/09/05.

36. Stegen S, Rinaldi G, Loopmans S, Stockmans I, Moermans K, Thienpont B, et al. Glutamine Metabolism Controls Chondrocyte Identity and Function. Dev Cell. Jun 8 2020;53(5):530-44 e8. Epub 2020/05/30.

37. Jilka RL. Molecular and cellular mechanisms of the anabolic effect of intermittent PTH. Bone. Jun 2007;40(6):1434-46. Epub 2007/05/23.

This article is protected by copyright. All rights reserved.

Accepted Article

38. Esen E, Lee SY, Wice BM, Long F. PTH Promotes Bone Anabolism by Stimulating Aerobic Glycolysis via IGF Signaling. J Bone Miner Res. Nov 2015;30(11):1959-68. Epub 2015/05/21.

39. Karner CM, Long F. Wnt signaling and cellular metabolism in osteoblasts. Cell Mol Life Sci. May 2017;74(9):1649-57. Epub 2016/11/27.

40. Stine ZE, Walton ZE, Altman BJ, Hsieh AL, Dang CV. MYC, Metabolism, and Cancer. Cancer Discov. Oct 2015;5(10):1024-39. Epub 2015/09/19.

41. Csibi A, Fendt SM, Li C, Poulogiannis G, Choo AY, Chapski DJ, et al. The mTORC1 pathway stimulates glutamine metabolism and cell proliferation by repressing SIRT4. Cell. May 9 2013;153(4):840-54. Epub 2013/05/15.

42. Onyia JE, Bidwell J, Herring J, Hulman J, Hock JM. In vivo, human parathyroid hormone fragment (hPTH 1-34) transiently stimulates immediate early response gene expression, but not proliferation, in trabecular bone cells of young rats. Bone. Nov 1995;17(5):479-84. Epub 1995/11/01.

43. Manolagas SC. From estrogen-centric to aging and oxidative stress: a revised perspective of the pathogenesis of osteoporosis. Endocr Rev. Jun 2010;31(3):266-300. Epub 2010/01/07.

44. Domazetovic V, Marcucci G, Iantomasi T, Brandi ML, Vincenzini MT. Oxidative stress in bone remodeling: role of antioxidants. Clin Cases Miner Bone Metab. May-Aug 2017;14(2):209-16. Epub 2017/12/22.

45. Jilka RL, Almeida M, Ambrogini E, Han L, Roberson PK, Weinstein RS, et al. Decreased oxidative stress and greater bone anabolism in the aged, when compared to the young, murine skeleton with parathyroid hormone administration. Aging Cell. Oct 2010;9(5):851-67. Epub 2010/08/12.

This article is protected by copyright. All rights reserved.

Accepted Article

Figure titles and legends

Figure 1. Exogenous glutamine is critical for osteoprogenitor function *in vitro*

A Schematic representation of experimental setup. Osterix (*Osx*)-GFP positive cells were isolated from 4-week-old *Osx*-GFP:Cre^{+} transgenic mice. Mice were maintained on doxycycline (Dox) from conception to weaning and cells were collected one week after Dox withdrawal.

B-C Proliferation (**B**) and cell viability (**C**) of sorted *Osx*-GFP positive cells cultured in decreasing glutamine concentrations, as analyzed by BrdU incorporation and Annexin V – propidium iodide flow cytometry, respectively (n=4).

D Picrosirius red (PSR), alkaline phosphatase (ALP) and Alizarin Red (AR) staining of *Osx*-GFP positive cells cultured in osteogenic differentiation medium with decreasing glutamine concentrations (n=4).

Data are presented as box-plot with indication of median; whiskers represent min to max values, $^{\#}p<0.05$ (ANOVA).

Figure 2. Deletion of GLS1 in osteoprogenitors impairs bone mass accrual

A Schematic representation of experimental setup. *Gls1*$^{ob+}$, *Gls1*^{ctrl} and *Gls1*$^{ob-}$ mice were sacrificed at 8 weeks of age. Mice were maintained on Dox from conception to weaning and experiments were performed 5 weeks after Dox withdrawal. For more information on the transgenic mouse models, we refer to Supplemental Figure 1.

B GLS1 and β-actin immunoblot on whole-cell extracts from total bone, *Osx*-GFP positive cells and periosteum-derived cells (PDC) (n=3). Cell extracts from total bone and PDC were isolated from *Gls1*$^{ob+}$ and *Gls1*$^{ob-}$ mice. *Osx*-GFP positive cells were isolated from *Gls1*^{ctrl} (*Osx*-GFP:Cre^{+}) and *Gls1*$^{ob-}$ mice.

C-E 3D microCT models of the tibial metaphysis (top) and diaphysis (bottom) (**C**) and quantification of trabecular bone volume (BV/TV; **D**) and cortical thickness (Ct.Th; **E**) in *Gls1*$^{ob+}$ and *Gls1*$^{ob-}$ mice (n=8).

This article is protected by copyright. All rights reserved.

Accepted Article

F-G H&E staining of the tibial metaphysis (**F**) with quantification (**G**) of osteoblast number per bone surface (N.Ob/B.S) in *Gls1*$^{ob+}$ and *Gls1*$^{ob-}$ mice (n=8). Black arrowheads in (**F**) indicate osteoblasts.

H-J Calcein labeling showing mineralizing surfaces on metaphyseal trabeculae (**H**) with quantification of the bone formation rate (BFR; **I**) and mineral apposition rate (MAR; **J**) in *Gls1*$^{ob+}$ and *Gls1*$^{ob-}$ mice (n=8). White arrowheads in (**H**) indicate calcein incorporation.

K Serum osteocalcin levels in *Gls1*$^{ob+}$ and *Gls1*$^{ob-}$ mice (n=8)

L-M TRAP staining of the tibial metaphysis (**L**) with quantification (**M**) of osteoclast surface per bone surface (Oc.S/B.S) in *Gls1*$^{ob+}$ and *Gls1*$^{ob-}$ mice (n=8). Black arrowheads in (**L**) indicate osteoclasts.

N Serum CTx-I levels in *Gls1*$^{ob+}$ and *Gls1*$^{ob-}$ mice (n=8).

Scale bars are 100 µm. Data are presented as box-plot with indication of median; whiskers represent min to max values, *p<0.05 vs *Gls1*$^{ob+}$, ***p<0.001 vs *Gls1*$^{ob+}$ (Student's *t*-test).

Figure 3. GLS1 inactivation in osteoprogenitors impairs glutamine flux into biosynthetic and redox pathways

A Schematic representation of experimental setup. *Osx*-GFP positive cells were isolated from 4-week-old *Gls1*^{ctrl} and *Gls1*$^{ob-}$ mice. Mice were maintained on Dox from conception to weaning and cells were collected one week after Dox withdrawal. For more information on the transgenic mouse models, we refer to Supplemental Figure 1.

B Proliferation of sorted *Osx*-GFP positive cells from *Gls1*^{ctrl} and *Gls1*$^{ob-}$ mice, as determined by BrdU incorporation (n=4).

C-D Cell viability (**C**) and intracellular ROS levels (**D**) of sorted *Osx*-GFP positive cells from *Gls1*^{ctrl} and *Gls1*$^{ob-}$ mice, analyzed by Annexin V – propidium iodide and CellROX flow cytometry, respectively (n=4).

E Picrosirius Red (PSR), alkaline phosphatase (ALP) and Alizarin Red (AR) staining of sorted *Osx*-GFP positive cells from *Gls1*^{ctrl} and *Gls1*$^{ob-}$ mice, cultured in osteogenic differentiation medium (n=4).

This article is protected by copyright. All rights reserved.

Accepted Article

F Schematic representation of $^{13}C_5$-glutamine tracing. Filled circles indicate ^{13}C, and open circles denote ^{12}C. Ac-Coa is acetyl-CoA, αKG is α-ketoglutarate, GSH is reduced glutathione.

G-P Isotopic labeling of glutamate (**G**), αKG (**H**), succinate (**I**), fumarate (**J**), malate (**K**), citrate (**L**), aspartate (**M**), proline (**N**), UMP (**O**) and GSH (**P**) from $^{13}C_5$-glutamine in sorted *Osx*-GFP positive cells from *Gls1*^{ctrl} and *Gls1*$^{ob-}$ mice (n=4). Specific mass distribution vectors (MDV) for each metabolite are shown.

Q Intracellular αKG, succinate (Suc), fumarate (Fum), citrate (Cit), glutamate (Glu), asparate (Asp), proline (Pro), UMP and GSH levels in sorted *Osx*-GFP positive cells from *Gls1*^{ctrl} and *Gls1*$^{ob-}$ mice (n=4).

Data are presented as box-plot with indication of median; whiskers represent min to max values. In **Q**, data are presented as mean values. *p<0.05 vs *Gls1*^{ctrl}, **p<0.01 vs *Gls1*^{ctrl}, ***p<0.001 vs *Gls1*^{ctrl} (Student's *t*-test).

Figure 4. Metabolic rescue of functional defects in GLS1-deficient osteoprogenitors

A Proliferation of sorted *Osx*-GFP positive cells with or without supplementation of non-essential amino acids (NEAA) and nucleotides (nucl) as analyzed by BrdU incorporation (n=4). *Osx*-GFP positive cells were isolated from 4-week-old *Gls1*^{ctrl} and *Gls1*$^{ob-}$ mice. Mice were maintained on Dox from conception to weaning and cells were collected one week after Dox withdrawal. For more information on the transgenic mouse models, we refer to Supplemental Figure 1.

B Picrosirius Red (PSR), alkaline phosphatase (ALP) and Alizarin Red (AR) staining of sorted *Osx*-GFP positive cells from *Gls1*^{ctrl} and *Gls1*$^{ob-}$ mice, cultured in osteogenic differentiation medium with or without NEAA supplementation (n=4).

C-D Protein synthesis (**C**) and collagen synthesis (**D**) of sorted *Osx*-GFP positive cells from *Gls1*^{ctrl} and *Gls1*$^{ob-}$ mice with or without NEAA supplementation (n=3).

This article is protected by copyright. All rights reserved.

Accepted Article

E Intracellular α-ketoglutarate (αKG), succinate (Suc), fumarate (Fum), malate (Mal), citrate (Cit), glutamate (Glu), aspartate (Asp), proline (Pro), UMP and reduced glutathione (GSH) levels in sorted *Osx*-GFP positive cells from *Gls1*^{ctrl} and *Gls1*$^{ob-}$ mice with or without αKG supplementation (n=4).

F-H Proliferation (**F**), protein synthesis (**G**) and collagen synthesis (**H**) of sorted *Osx*-GFP positive cells from *Gls1*^{ctrl} and *Gls1*$^{ob-}$ mice with or without αKG supplementation (n=3-4).

I PSR, ALP and AR staining of sorted *Osx*-GFP positive cells from *Gls1*^{ctrl} and *Gls1*$^{ob-}$ mice, cultured in osteogenic differentiation medium with or without αKG supplementation (n=4).

J-K Intracellular ROS levels (**J**) and cell viability (**K**) of sorted *Osx*-GFP positive cells from *Gls1*^{ctrl} and *Gls1*$^{ob-}$ mice, with or without glutathione ethyl ester (GSH-EE) supplementation, as analyzed by CellROX flow cytometry and Annexin V – propidium iodide, respectively (n=4).

Data are presented as box-plot with indication of median; whiskers represent min to max values. In **E**, data are presented as mean values. $^{\#}p<0.05$, °$p<0.05$ vs *Gls1*^{ctrl} without αKG, $^{\S}p<0.05$ vs *Gls1*$^{ob-}$ without αKG (ANOVA).

Figure 5. PTH treatment enhances glutamine metabolism in osteoprogenitors

A Schematic representation of experimental setup. *Osx*-GFP positive cells were sorted from 4-week-old *Osx*-GFP:Cre^{+} transgenic mice. Mice were maintained on Dox from conception to weaning, cells were collected one week after Dox withdrawal, and subsequently treated with PTH for 48 hours.

B *Slc1a5*, *Slc38a1*, *Slc38a3*, *Gls1* and *Glud1* mRNA levels in Osx-GFP positive cells treated with PTH at different concentrations (n=4).

C SLC1A5, GLS1 and β-actin immunoblot on whole-cell extracts from vehicle (veh) and PTH-treated *Osx*-GFP positive cells (n=3).

D Glutamine (Gln) uptake of veh and PTH-treated *Osx*-GFP positive cells (n=4).

This article is protected by copyright. All rights reserved.

Accepted Article

E-N Isotopic labeling of glutamate (**E**), αKG (**F**), succinate (**G**), fumarate (**H**), malate (**I**), citrate (**J**), aspartate (**K**), proline (**L**), GSH (**M**) and UMP (**N**) from $^{13}C_5$-glutamine in veh and PTH-treated *Osx*-GFP positive cells (n=4). Specific mass distribution vectors (MDV) for each metabolite are shown.

O Intracellular α-ketoglutarate (αKG), succinate (Suc), fumarate (Fum), malate (Mal), citrate (Cit), glutamate (Glu), aspartate (Asp), proline (Pro), UMP and reduced glutathione (GSH) levels in veh and PTH-treated *Osx*-GFP positive cells (n=4).

Data are presented as box-plot with indication of median; whiskers represent min to max values. In **B** and **O**, data are presented as mean values. *p<0.05 vs veh, **p<0.01 vs veh, ***p<0.001 vs veh (Student's *t*-test).

Figure 6. GLS1 inactivation in osteoprogenitors blunts PTH-induced glutamine catabolism *in vitro*

A Schematic representation of experimental setup. *Osx*-GFP positive cells were isolated from 4-week-old *Gls1*^{ctrl} and *Gls1*$^{ob-}$ mice. Mice were maintained on Dox from conception to weaning, cells were collected one week after Dox withdrawal, and subsequently treated with PTH for 48 hours. For more information on the transgenic mouse models, we refer to Supplemental Figure 1.

B Glutamine (Gln) uptake in vehicle (-) and PTH-treated *Osx*-GFP positive cells from *Gls1*^{ctrl} and *Gls1*$^{ob-}$ mice (n=4).

C Intracellular α-ketoglutarate (αKG), succinate (Suc), fumarate (Fum), malate (Mal), citrate (Cit), glutamate (Glu), aspartate (Asp), proline (Pro), UMP and reduced glutathione (GSH) levels in vehicle and PTH-treated *Osx*-GFP positive cells from *Gls1*^{ctrl} and *Gls1*$^{ob-}$ mice (n=4).

Data are presented as box-plot with indication of median; whiskers represent min to max values. In **C**, data are presented as mean values. $^{\#}$p<0.05, °p<0.05 vs *Gls1*^{ctrl}-vehicle, §p<0.05 vs *Gls1*^{ctrl}-PTH (ANOVA).

This article is protected by copyright. All rights reserved.

Accepted Article

Figure 7. GLS1 inactivation in osteoprogenitors impairs PTH-induced bone anabolism

A Schematic representation of experimental setup. *Gls1*$^{ob+}$ and *Gls1*$^{ob-}$ male mice were maintained on Dox until 8 weeks of age. One day after Dox withdrawal, mice were treated with PTH 5 times a week for 4 weeks (intermittent PTH; iPTH). For more information on the transgenic mouse models, we refer to Supplemental Figure 1.

B SLC1A5, GLS1 and β-actin immunoblot on metaphyseal bone cell extracts derived from vehicle (-) and PTH-treated *Gls1*$^{ob+}$ and *Gls1*$^{ob-}$ mice (n=3).

C-D 3D microCT models of the tibial metaphysis (**C**) and quantification of trabecular bone volume (BV/TV; **D**) in vehicle and PTH-treated *Gls1*$^{ob+}$ and *Gls1*$^{ob-}$ mice (n=7-8).

E-F H&E staining of the tibial metaphysis (**E**) with quantification (**F**) of osteoblast number per bone surface (N.Ob/B.S) in vehicle and PTH-treated *Gls1*$^{ob+}$ and *Gls1*$^{ob-}$ mice (n=7-8). Black arrowheads in (**E**) indicate osteoblasts.

G-I Goldner staining of the tibial metaphysis (**G**) with quantification of non-mineralized bone matrix (osteoid) surface per bone surface (O.S/B.S; **H**) and osteoid thickness (O.Th; **I**) in vehicle and PTH-treated *Gls1*$^{ob+}$ and *Gls1*$^{ob-}$ mice (n=7-8). Black arrowheads in (**G**) indicate osteoid.

J-K Calcein labeling of mineralizing surfaces on metaphyseal trabeculae (**J**) with quantification of the bone formation rate (BFR; **K**) in vehicle and PTH-treated *Gls1*$^{ob+}$ and *Gls1*$^{ob-}$ mice (n=7-8). White arrowheads in (**J**) indicate calcein incorporation.

L Serum osteocalcin levels in vehicle and PTH-treated *Gls1*$^{ob+}$ and *Gls1*$^{ob-}$ mice (n=7-8).

Scale bars are 100 μm. Data are presented as box-plot with indication of median; whiskers represent min to max values, $^{\#}p<0.05$ (ANOVA).

This article is protected by copyright. All rights reserved.

Accepted Article

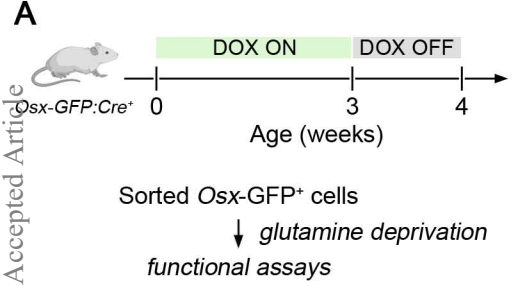

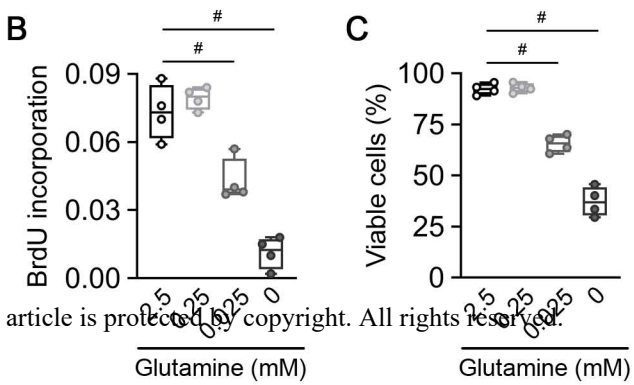

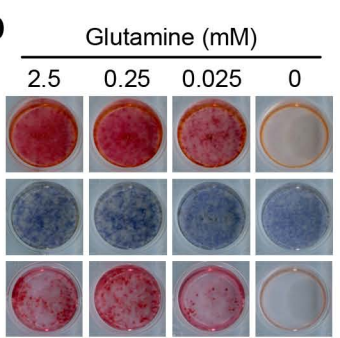

This article is protected by copyright. All rights reserved.

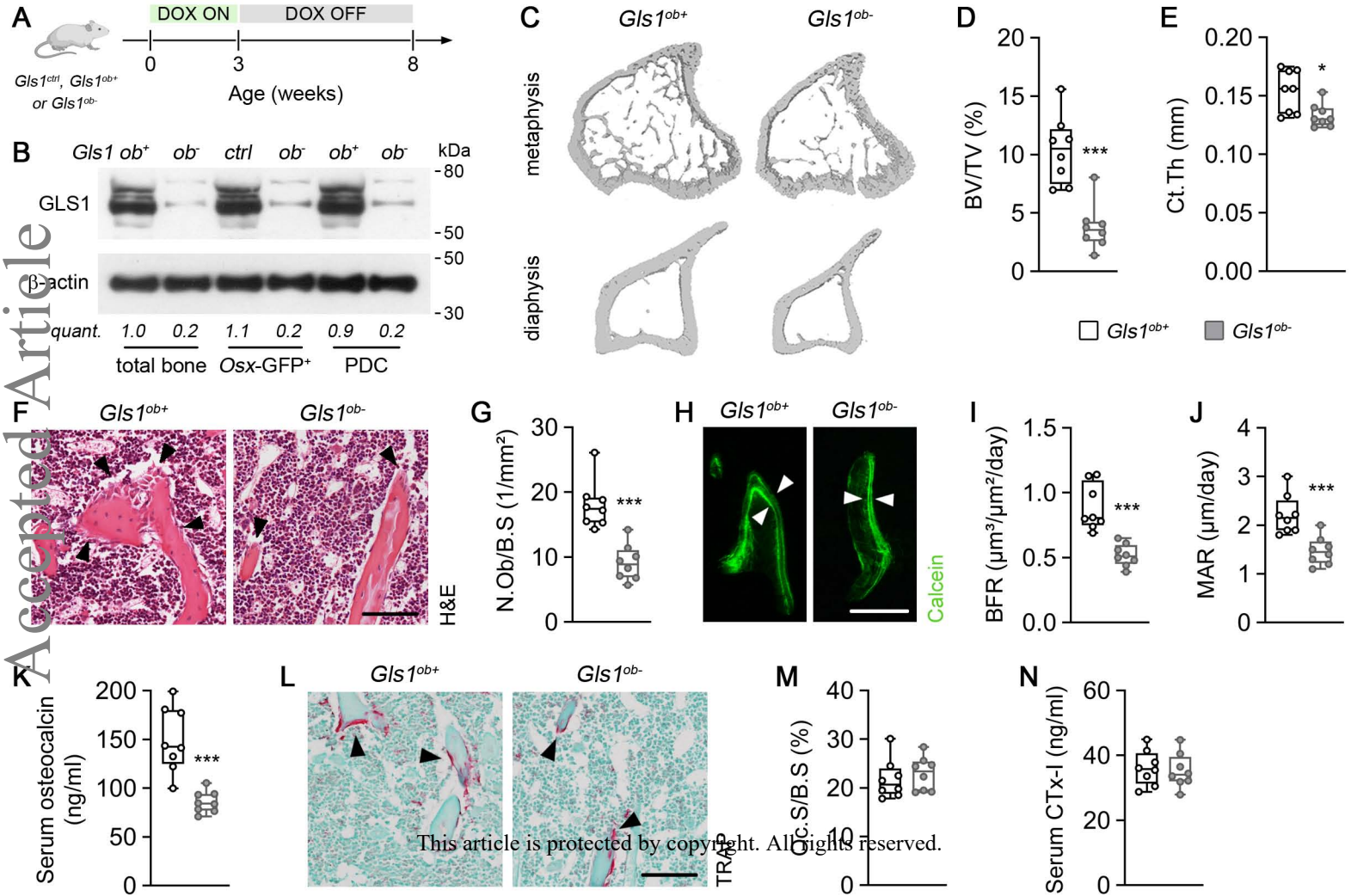

Accepted Article

This article is protected by copyright. All rights reserved.

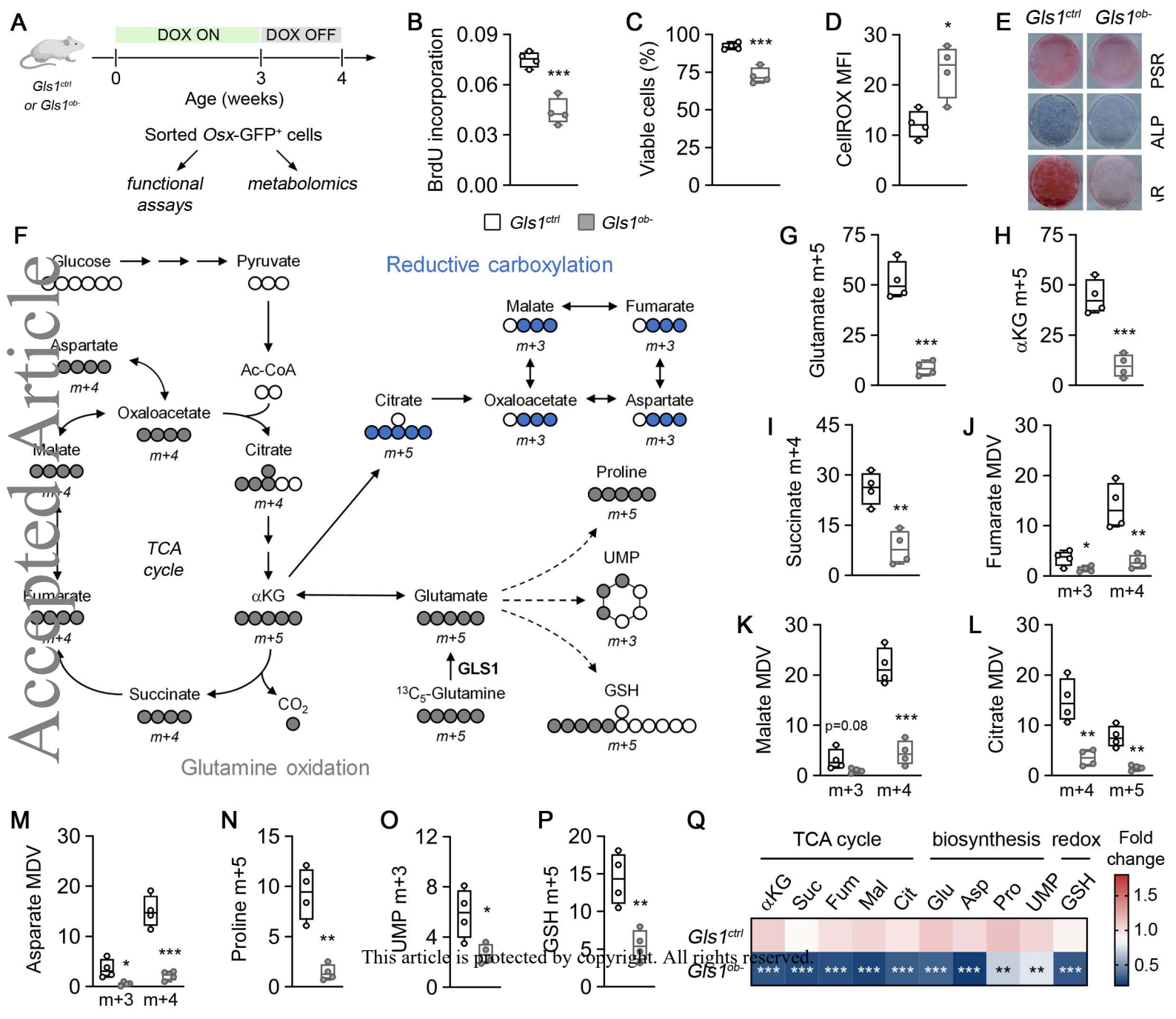

Accepted Article

This article is protected by copyright. All rights reserved.

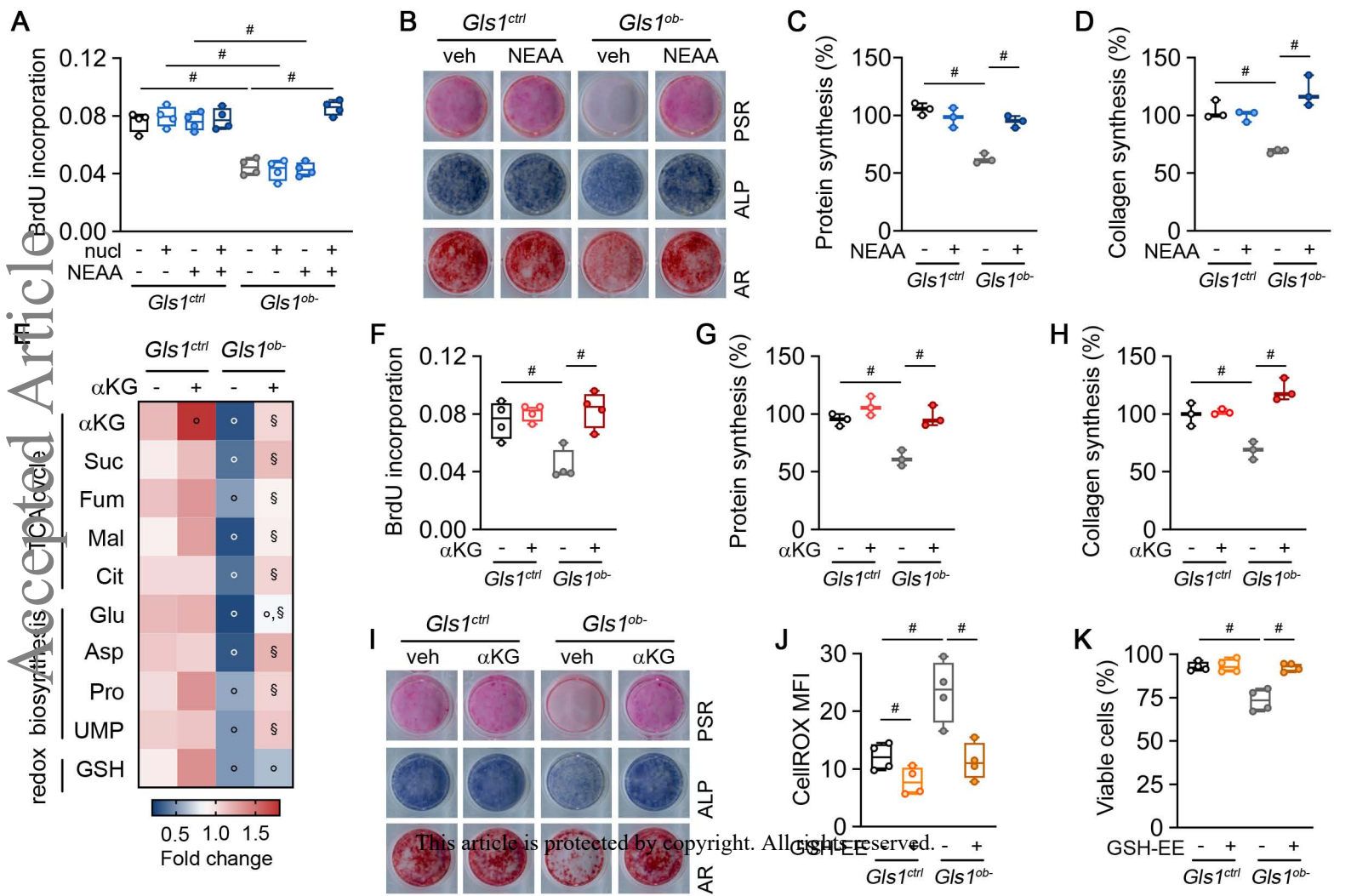

Accepted Article

This article is protected by copyright. All rights reserved.

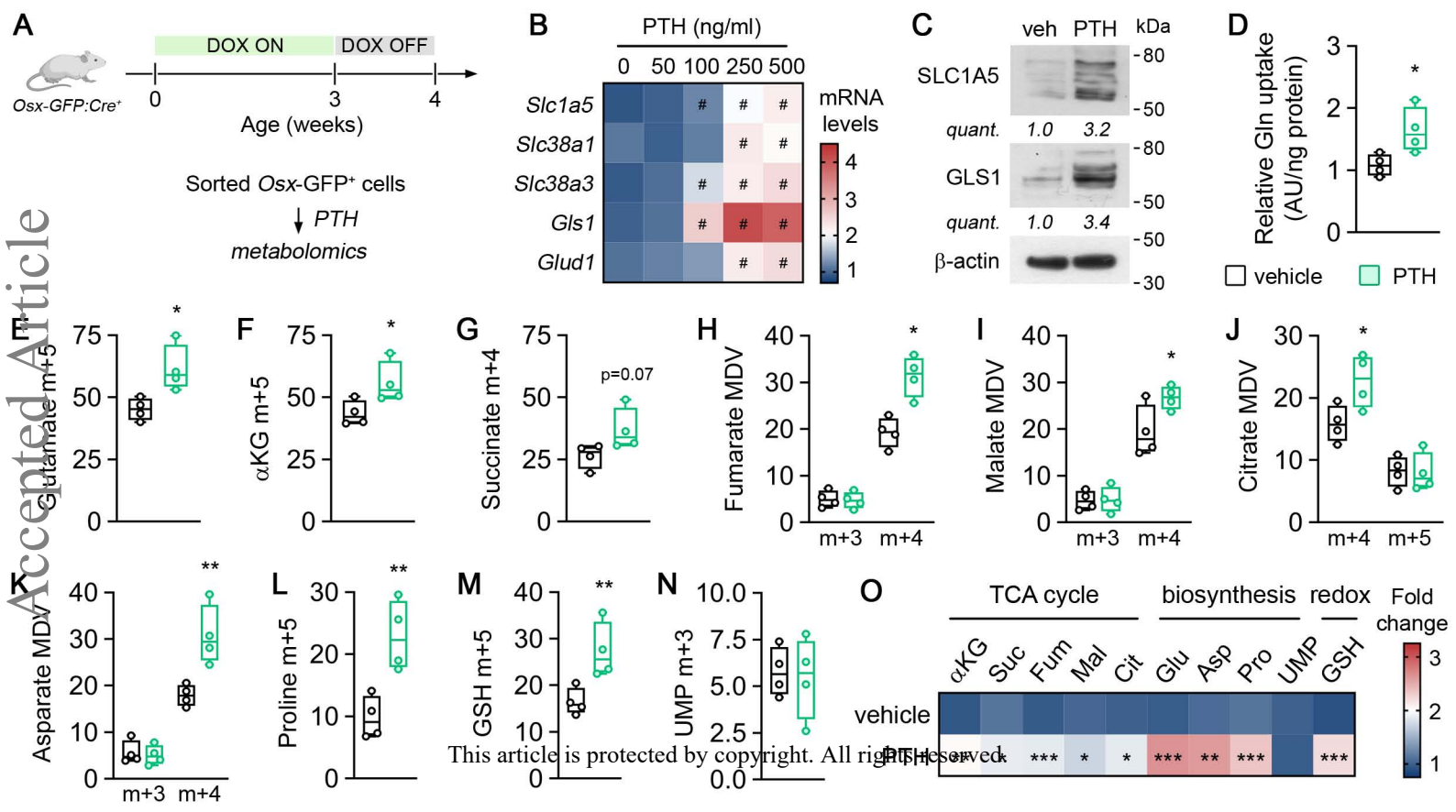

Accepted Article

This article is protected by copyright. All rights reserved.

Accepted Article

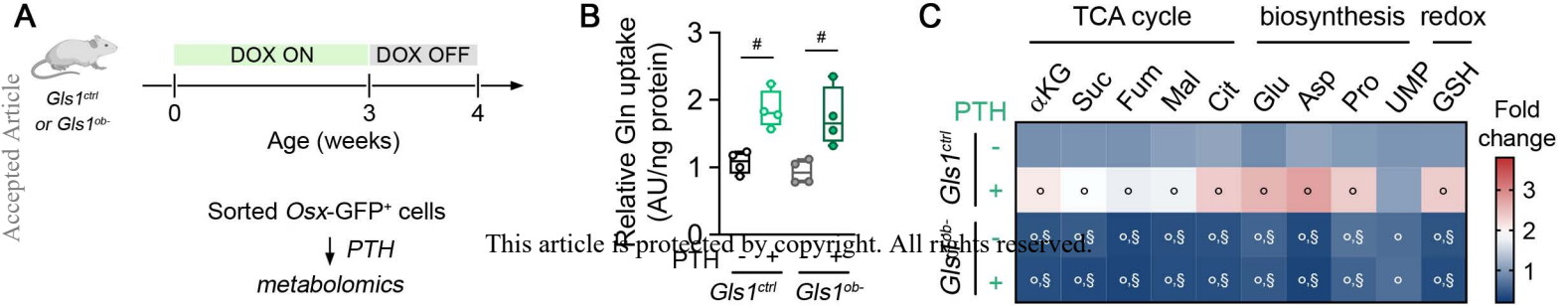

This article is protected by copyright. All rights reserved.

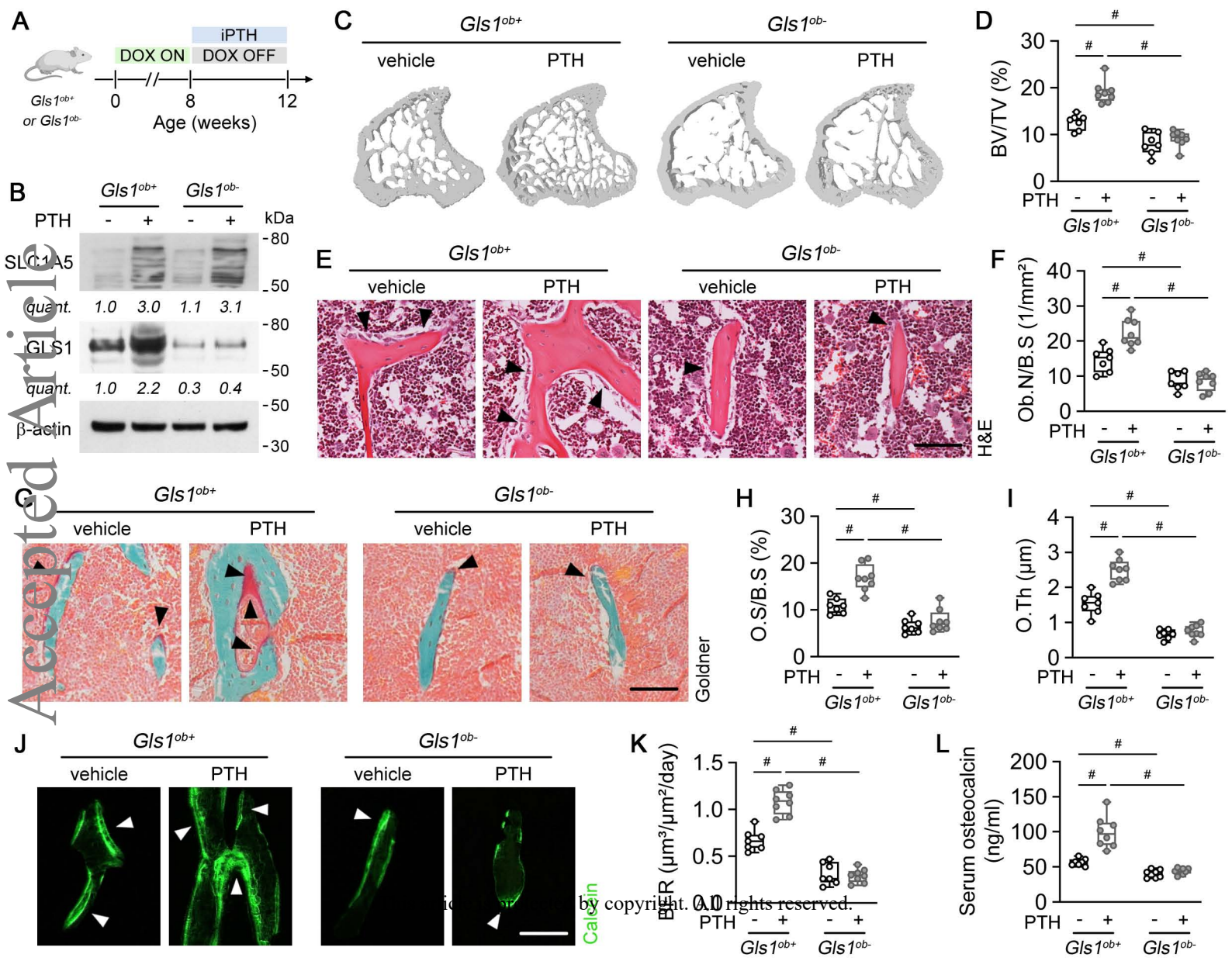

Accepted Article

by copyright. All rights reserved.